

Sparse Spike Encoding of Channel Responses for Energy Efficient Human Activity Recognition

Eleonora Cicciarella*, Riccardo Mazzieri, Jacopo Pegoraro, Michele Rossi

Abstract—ISAC enables pervasive monitoring, but modern sensing algorithms are often too complex for energy-constrained edge devices. This motivates the development of learning techniques that balance accuracy performance and energy efficiency. Spiking Neural Networks (SNNs) are a promising alternative, processing information as *sparse* binary spike trains and potentially reducing energy consumption by orders of magnitude.

In this work, we propose a spiking convolutional autoencoder (SCAE) that learns tailored spike-encoded representations of channel impulse responses (CIR), jointly trained with an SNN for human activity recognition (HAR), thereby eliminating the need for Doppler domain preprocessing. The results show that our SCAE-SNN achieves F1 scores comparable to a hybrid approach (almost 96%), while producing substantially sparser spike encoding (81.1% sparsity). We also show that encoding CIR data prior to classification improves both HAR accuracy and efficiency. The code is available at <https://github.com/ele-ciccia/SCAE-SNN-HAR>.

Index Terms—Spiking neural networks, edge computing, integrated sensing and communication, energy efficiency.

I. INTRODUCTION

Human Activity Recognition (HAR) has gained significant attention in recent years due to its wide range of applications in healthcare, smart homes, and related fields. Conventional HAR solutions can be broadly classified into *device-based* and *device-free*. Device-based methods, such as wearables and smartphones, are effective but often impractical for long-term use. Device-free approaches, on the other hand, remove the burden of carrying sensors and instead rely on the environment. Vision-based systems are a common example, though their adoption is hindered by privacy concerns and sensitivity to lighting and temperature conditions.

These limitations have accelerated interest in Radio Frequency (RF)-based HAR, which leverages the interaction between wireless signals and human movements [1]. Since RF signals are affected by reflection, diffraction, and scattering, they enable activity recognition without direct user involvement, thus preserving privacy. Moreover, RF-based HAR aligns with the emerging Integrated Sensing and Communication (ISAC) paradigm, where communication systems are extended with sensing capabilities. A key element in this setting is the Channel Impulse Response (CIR), which inherently captures variations in the wireless channel induced by human motions, offering a rich source of information

for activity recognition. In particular, the use of millimeter waves (mmWave) ISAC systems enhances sensing by providing higher temporal and spatial resolution through their large bandwidths and short wavelengths, resulting in clearer echo signatures and improved resolution of fine-grained human motions that are difficult to resolve at lower frequencies.

Due to the complexity of such channel, Deep Learning (DL) solutions are commonly used to enable advanced sensing applications such as target recognition, movement analysis, and gesture recognition from Doppler spectrograms or range-Doppler maps [2], [3]. Although effective, these approaches incur high computational cost due to data volume and DL inference, hindering the implementation on resource-constrained edge devices and routers, where RF data are collected [4].

To overcome these challenges, Spiking Neural Networks (SNNs) [5] have recently gained attention for edge computing applications. Unlike standard Artificial Neural Networks (ANNs) which process dense values through energy-hungry multiply-accumulate (MAC) operations, SNNs encode information into *sparse spike trains* and operate with lightweight accumulate (AC) operations. Their event-driven processing offers orders-of-magnitude energy savings and has already been validated on neuromorphic hardware [6].

In this work, we propose an end-to-end processing pipeline leveraging SNNs to perform HAR directly from raw CIR data, thus avoiding the need for heavy Doppler-domain preprocessing. Specifically, the main contributions are:

- 1) We propose a *learned* spike encoding tailored to CIR data, balancing activity recognition accuracy and spike sparsity. Our SNN classifier trained on the proposed learned encoding achieves the highest F1 score ($\approx 96\%$) among competing approaches, including the Convolutional Autoencoder (CAE), SNN with no-encoding, and encoding via fixed delta thresholding. Moreover, our approach produces the sparsest spike representation, with 81.1% sparsity compared to 28.6% and 71.7 % for the CAE and delta thresholding methods, respectively.
- 2) The proposed spike-based architecture effectively learns spectral features relevant to classification directly from CIRs, whereas a standard deep Convolutional Neural Network (CNN) originally trained on Doppler spectrograms experiences a performance drop of about 10 percentage points when trained on raw CIR data.

The paper is organized as follows. Section II reviews related work on RF-based HAR. Section III introduces the necessary background on wireless channel modeling and the Leaky Integrate and Fire (LIF) spiking neuron model. The dataset and preprocessing steps are described in Section IV, while

*Corresponding author eleonora.cicciarella@phd.unipd.it. All authors are with the University of Padova, Department of Information Engineering. This work was partially supported by the European Union under the Italian National Recovery and Resilience Plan (NRRP) Mission 4, Component 2, Investment 1.3, CUP C93C22005250001, partnership on “Telecommunications of the Future” (PE00000001 - program “RESTART”).

the proposed models and methods are detailed in Section V. Section VI presents and discusses the experimental results. Finally, Section VII concludes the paper with a summary of findings and future research directions.

II. RELATED WORK

Radar-based HAR has relied on classical signal processing for feature extraction coupled with machine learning classifiers [7], or, more recently, on DL architectures [8]. To overcome the computational complexity and energy consumption of DL, which hinders its deployment on resource-constrained devices, researchers have increasingly shifted to SNNs. Their sparse and event-driven computations offer significant advantages in energy efficiency. One of the first studies in this direction is [9], where the authors design a convolutional SNN to capture temporal dynamics in radar micro-Doppler signatures for HAR. Subsequent research has largely focused on the more specific task of gesture recognition. The authors of [10] propose a recurrent SNN based on liquid state machines (LSMs) to classify range-Doppler (RD) and micro-Doppler (μ D) radar signals, using a signal-to-spike conversion scheme to encode them into spike trains. In [11], a three-layer SNN with LIF neurons is utilized to recognize four hand gestures from RD maps. The above works all share one main limitation, i.e., they rely on standard radar signal processing to obtain RD or μ D maps, which are then encoded into spike sequences. This approach does not fully exploit the sparsity of the radio channel features, since it processes high-dimensional tensors that mostly contain zeros at high computation and energy cost. Conversely, in this paper, we make the SNN *learn directly from the raw CIR*, without inefficient preprocessing steps.

To the best of our knowledge, only works [12], [13] have addressed HAR from raw Analog-to-Digital Converter (ADC) or CIR data, using a convolutional SNN and a hybrid CNN-SNN, respectively. However, in [12] the SNN is partially constrained to mimic the Discrete Fourier Transform (DFT) computation in standard radar processing, reducing its learning capabilities. Moreover, the *spike activity* of the proposed network, i.e., the percentage of time in which the network neurons emit a spike, is not analyzed nor compared to other SNN models. On the contrary, [13] requires a standard CNN block to perform spike encoding, which shares the high energy consumption of standard DL. Conversely, we design an *end-to-end* SNN comprising an encoder module that specifically learns to produce tailored spike trains to preserve human movement features, while minimizing spike activity for low energy operation.

III. BACKGROUND

A. Wireless channel modeling

The estimation of the CIR plays a central role in radar and ISAC systems, as it embeds information about the location and movement of objects and people [2]. The CIR is represented as a vector of complex channel gains, also referred to in the following as *paths*, each characterized by an amplitude and a phase. Due to the finite delay resolution of the system,

the CIR vector can only represent a discrete set of paths $\ell = 0, \dots, L-1$, each characterized by a propagation delay $\tau_\ell = \ell/B$, where B denotes the transmission bandwidth and $1/B$ corresponds to the delay resolution. Assuming an analog beamforming system is used, multiple CIR estimations per packet can be obtained using different beam-patterns (BPs). The CIR obtained with each BP encodes different environmental reflections, due to the different BP shapes. Repeating the CIR estimation for each packet k effectively samples the channel over time, with sampling period corresponding to the inter-packet transmission time T_c . For a given BP p and time instant (packet) k , the ℓ -th component of the CIR can be written as

$$h_{\ell,p}[k] \triangleq h_{\ell,p}(kT_c) = a_{\ell,p}(kT_c) e^{j\phi_\ell(kT_c)}, \quad (1)$$

where $a_{\ell,p}(k)$ and $\phi_\ell(k)$ represent the complex gain and phase of path ℓ at time k , respectively. The path gain depends on the contribution of the BP used for the transmission and on the reflectivity of the target, while the phase depends on the delay.

B. Spiking neuron model

Various spiking neuron models have been proposed that strike a good balance between biological plausibility and computational practicality. In this work, we adopt the LIF neuron model [14], which is widely used in learning applications due to its simplicity and fidelity in mimicking the behavior of biological neurons. Each LIF neuron is characterized by an internal state called *membrane potential*, acting as a leaky integrator of the input signal. SNNs are constituted by a network of LIF neurons, typically organized into layers. Denoting by $U_i^{(\ell)}(t)$ the membrane potential of the i -th neuron in layer ℓ at time t , R the input resistance, and $I_i^{(\ell)}(t)$ the input current to the neuron at time t , the dynamics of the membrane potential over time are described by the following differential equation:

$$\tau \frac{dU_i^{(\ell)}(t)}{dt} = -U_i^{(\ell)}(t) + RI_i^{(\ell)}(t), \quad (2)$$

where τ is the membrane time constant. Whenever the membrane potential exceeds a predefined threshold θ , the neuron emits a unitary *spike* $S_i^{(\ell)}$, and $U_i^{(\ell)}$ is instantaneously reset to a resting value. Assuming $R = 1\Omega$ and accounting for spiking and membrane potential reset, we formulate the above equation in discrete time using Euler's approximation method:

$$U_i^{(\ell)}[t] = \beta \cdot U_i^{(\ell)}[t-1] + I_i^{(\ell)}[t] - \theta \cdot S_i^{(\ell)}[t-1] \quad (3)$$

$$I_i^{(\ell)}[t] = \sum_j W_{ij}^{(\ell)} S_j^{(\ell-1)}[t] \quad (4)$$

$$S_i^{(\ell)}[t] = \Theta(U_i^{(\ell)}[t] - \theta), \quad (5)$$

where $\beta = e^{-1/\tau}$ represents the decay rate of the membrane potential in the absence of input stimuli, and the input current is represented as a weighted sum of the incoming spikes. Eq. (5) defines the spike generation mechanism, where $\Theta(\cdot)$ denotes the Heaviside step function.

IV. DATASET

Overview: The DISC dataset [15] provides CIR measurements from standard-compliant IEEE 802.11ay packets, intended to support the evaluation of ISAC methods. The CIR sequences capture signal reflections caused by human movement within a controlled, indoor environment characterized by complex multipath fading, due to the presence of furniture, computer equipment, display screens, and a large whiteboard. The data were collected using a 60 GHz software-defined radio experimentation platform based on the IEEE 802.11ay Wi-Fi standard, which is not affected by frequency offsets due to its monostatic full-duplex operation mode. The dataset comprises approximately 40 minutes of CIR recordings, capturing reflections from 7 subjects performing $N_C = 4$ different activities: *walking*, *running*, *sitting down/standing up*, and *waving hands*. See [15] for further details on the data acquisition process and experimental setup.

Preprocessing: Each record in the dataset represents a CIR sequence consisting of 110 range bins, where each bin corresponds to a specific time delay, i.e., a specific distance from the transmitter, and the total length of the sequences may vary depending on the duration of the measurement. Before being fed into the network, each complex-valued CIR sequence is segmented into partially overlapping time windows of length $W = 64$ samples with step size $\delta = 32$, providing short-term snapshots of the channel evolution. Within each window, the real and imaginary components are extracted, and the moving interquartile range (IQR) is computed along slow time to quantify temporal variability. The IQRs of the real and imaginary parts are combined into a joint measure, and the top $R = 10$ range bins with the highest variability are selected, ensuring that only the most dynamic and informative portions of the CIR are retained as input features. Both the real and imaginary parts of the CIR are preserved to fully retain the channel amplitude and phase information, the latter being particularly important as it encodes subtle variations induced by the human motion. Finally, each CIR is normalized to the range $[0, 1]$ using min-max normalization.

Notably, the information critical for classification is concentrated within about 2 – 3 seconds of data, corresponding to approximately $N = 232$ windows, when considering a sampling time $T_c = 0.27$ ms. For this reason, sequences with a higher number of windows are divided into overlapping segments of length N , with an overlap of $N/2$ windows. This strategy enables the generation of additional samples from the same recorded sequence. Furthermore, it introduces temporal variability and partially incomplete activity patterns, which act as a regularizer during training and improve the robustness of the model to temporal uncertainty. Instead, sequences with a smaller number of windows are discarded, as they may not contain enough information to recognize the activity. As a result, after preprocessing, each sample has shape $(2, N, R, W)$, where the 2 represents the real and imaginary components and will be treated as the input channel dimension for convolutional layers.

We included CIR sequences from subjects 1–4 and subject 6 in the training set, while subjects 5 and 7 are used for the validation and test sets, respectively. This ensures that every activity is represented at least once in each set and allows us to assess the generalization capability of the classifier to unseen subjects. The split yields 1,680, 138, and 182 elements in the training, validation, and test sets, respectively.

V. MODELS AND METHODS

This section presents the proposed methodology. Our architecture consists of a **convolutional autoencoder** with LIF neurons, hereafter referred to as *Spiking Convolutional Autoencoder (SCAE)*, used in combination with an SNN. The SCAE is responsible for extracting a spike-based representation of the input data, while the SNN performs the recognition of four distinct human activities, acting as a classifier. These two components are *jointly trained* in an end-to-end fashion: the SCAE is optimized to minimize the reconstruction error between the input CIR sample and its reconstruction, while the SNN is trained to maximize the classification accuracy. By adding the SNN block, we push the encoder to output a spike representation that preserves important information about the movement. A detailed description of the architecture is provided in Section V-A.

To evaluate the effectiveness of the proposed spike encoding, we compare it with the following alternative strategies:

- Convolutional autoencoder (CAE):* this variant replaces the SCAE block of the proposed architecture with a CAE with standard artificial neurons, as proposed in [13] (Section V-B).
- Delta thresholding encoding:* spike trains are generated using a thresholding mechanism (see Section V-C) based on the temporal structure and variability of the input signal. Hence, such spikes are fed into our SNN classifier.
- Plain CIR processing (Direct-SNN):* we also consider a baseline where no encoding is applied. CIR samples are directly fed into an SNN classifier, treating the input as a continuous current (see Section V-D).

A. SCAE-SNN architecture

The proposed learning-based encoding method tailored to CIR samples is shown in Fig. 1. The structure of the encoder-decoder block (SCAE) and the SNN follows the implementation described in [13] with appropriate modifications. In the following we provide a detailed description of each block.

SCAE: The SCAE is composed of an *encoder* that takes as input the CIR samples and outputs the corresponding spike encoding. The latter is then fed into the *decoder*, to reconstruct the original input. In the proposed architecture, the encoder employs two three-dimensional convolutional layers (Conv3D), each of them followed by batch normalization and a dense layer of LIF neurons. The convolutional layers have 64 and 2 feature maps, respectively, and extract local spectral patterns in the input data using a kernel of dimension $1 \times 1 \times 3$. A stride of 1 and zero padding are employed to preserve the input dimension. The LIF neurons are initialized with a decay

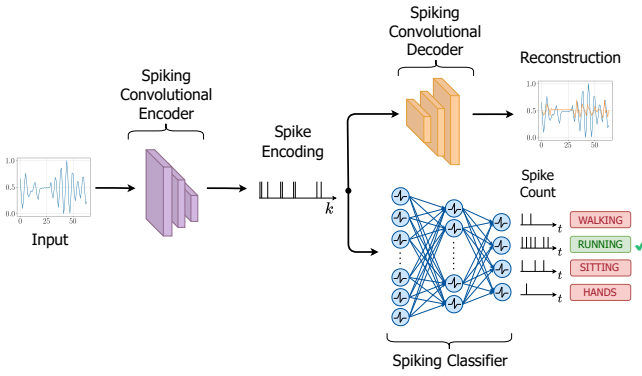


Figure 1: Block diagram of the proposed SCAE-SNN architecture.

factor $\beta = 0.9$ and a threshold $\theta = 1$. To provide greater flexibility, both parameters are then refined during training. Although the encoder does not perform dimensionality reduction, it compresses the CIR by binarizing its values. This introduces information loss, preventing the autoencoder from simply learning the identity function.

The decoder block approximately inverts the operations performed by the encoder to reconstruct the CIR sample. It employs 2 transposed Conv3D layers with 64 and 2 feature maps, respectively. Similarly to the encoder, the first transposed Conv3D layer is followed by batch normalization and a layer of LIF neurons. In contrast, the second one uses a standard sigmoid activation, since the input is normalized within $[0, 1]$. The remaining parameters are the same as those used in the encoder. Finally, the SCAE is trained for $T = 2$ timesteps, with each timestep processing a fixed sequence of $N/T = 116$ consecutive input windows.

SNN: The SNN classifier receives the spike encoding and predicts human activity. The encoding is first downsampled by average pooling (kernel $1 \times 1 \times 4$ and stride $1 \times 2 \times 2$), then processed by three fully connected layers with 128, 64, and N_C LIF neurons, respectively. The decay factor β and the firing threshold θ are initialized with values 0.9 and 0.8, respectively, and are refined during training, except for the final classification layer which uses a fixed $\theta = 1$. The network is trained for 29 timesteps and the output spikes are interpreted using a *rate coding* scheme (further detailed in Section V-E).

B. CAE-SNN architecture

The CAE produces *bipolar* spikes (both positive and negative) using a custom Heaviside function centered at $\tau = 0.4$, as described in [13]. The CAE shares the same structure and parameters as the SCAE, except for the LIF neurons that are replaced by ReLU activation, and is jointly trained with the SNN previously described to minimize the reconstruction error and maximize the classification accuracy.

C. Delta thresholding encoding

Letting n be the n -th time sample, and m the m -th range bin, the delta filter for a single CIR sample is

$$x_\delta(n, m) = x(n, m) - x(n-1, m), \quad (6)$$

where this equation is independently applied to the real and imaginary parts of the CIR. Calling σ_i the variance of $x_\delta(i, m)$, for each $i = 1, \dots, W$, and $\alpha = \mathbb{E}[\sigma_i]$, the final spike encoding s is obtained by thresholding the x_δ as follows:

$$s(n, m) = \begin{cases} 1, & \text{if } x_\delta(n, m) > \alpha \\ -1, & \text{if } x_\delta(n, m) < -\alpha \\ 0, & \text{otherwise.} \end{cases} \quad (7)$$

Despite its simplicity, this method has been proven to be effective for RF data [16]. For a fair comparison of the different encoding strategies, the SNN of Section V-A is trained on the resulting spike trains to recognize human activities.

D. Direct-SNN

Two types of SNNs are evaluated for direct classification from CIRs. The first uses fully connected layers with either three ($64-128-N_c$) or four ($64-128-256-N_c$) layers, where input features are downsampled via average pooling as in Section V-A. The second type employs convolutional feature extractors with one, two, or three layers (kernel $1 \times 1 \times 3$, stride 1), followed by a linear readout, using the channel progression $64 \rightarrow 128 \rightarrow 256$. All models share the same number of timesteps ($T = 29$) and parameter configuration for β and θ as the SNN described in Section V-A. Section VI reports the best results for each type: *Direct-SNN-Lin* with four linear layers and *Direct-SNN-Conv* with three convolutional layers.

E. Training method

Next, we describe the training process for each architecture, starting with the output decoding strategy.

Output spike decoding: In this work, we interpret output spikes as rate encoded outputs. Specifically, let N_C denote the number of output classes, and let $S[t] \in \{0, 1\}^{N_C}$ be the spike train emitted by the output layer of the SNN at timestep t . We compute the spike count vector $c \in \mathbb{Z}^{N_C}$ by summing the spike trains over T time steps: $c = \sum_{t=0}^{T-1} S[t]$. The predicted class label \hat{y} is then determined by the index of the neuron with the highest spike count: $\hat{y} = \arg \max_i c_i$. Rate decoding offers error tolerance by distributing the information across multiple spikes, reducing the impact of individual spike failures on the final prediction. Additionally, the presence of more spikes enhances learning dynamics by providing a stronger gradient signal during backpropagation [5].

Loss function: Both SCAE-SNN and CAE-SNN architectures are trained end-to-end through the minimization of a loss function that depends on the output of the decoder and of the SNN. Specifically, let \mathbf{X} and $\hat{\mathbf{X}}$ be the input CIR measurement and its reconstruction produced by the decoder, respectively. We define the reconstruction loss of the autoencoder using the Mean Squared Error (MSE) as $\mathcal{L}_{\text{rec}} \triangleq \text{MSE}(\mathbf{X}, \hat{\mathbf{X}})$. Moreover, let \mathbf{y} be the correct class and \mathbf{c} be the output spike count, as defined above. Then, we define the classification loss using the Cross-Entropy (CE) Spike Count as

$$\mathcal{L}_{\text{class}} = \sum_{i=0}^{N_C} y_i \log(p_i), \quad \text{with } p_i = \frac{e^{c_i}}{\sum_{j=1}^{N_C} e^{c_j}}. \quad (8)$$

Hence, the final loss for training both SCAE-SNN and CAE-SNN is given by $\mathcal{L} = \mathcal{L}_{\text{rec}} + \gamma \mathcal{L}_{\text{class}}$, with γ being a scaling parameter. All Direct-SNNs architectures are trained by minimizing $\mathcal{L}_{\text{class}}$ only.

To address class imbalance, we introduce weights in $\mathcal{L}_{\text{class}}$, chosen in $(0, 1]$ and selected via grid search. The weights are set inversely proportional to the class frequency and the classification difficulty, assigning lower values to common or easily recognized classes. Specifically, *walking* and *running* share a weight of 0.3, *sitting down* is assigned 0.6, and the most challenging class, *waving hands*, receives 1. Indeed, the latter only involves arm movements, which do not cause strong scattering of the radio signal and are hence difficult to detect.

Training and hyperparameter optimization: All architectures are trained with batches of 8 CIR samples, using back-propagation with Adam optimizer (learning rate $\eta = 10^{-4}$). To address the non-differentiability of the spike generation, we adopt the *surrogate gradient* approach [17] with the arctangent approximation of the firing threshold during the backward pass. Training is performed for a maximum of 50 epochs and is stopped if the validation F1 score does not improve for 15 consecutive epochs. Network hyperparameters are optimized through a grid search over a limited set of values, constrained by available resources, using validation loss as the objective. For the τ parameter of CAE, we performed five runs per candidate value to compute the mean and standard deviation of the encoding sparsity and classification accuracy on the validation set. Finally, we set $\gamma = 1$ in all experiments, as empirical observations showed that $\mathcal{L}_{\text{class}}$ consistently remained small compared to \mathcal{L}_{rec} , likely due to the high sparsity of spike-encoded data.

VI. EXPERIMENTAL RESULTS

In this section, we compare the spike encodings produced by SCAE, CAE, and delta thresholding for human activity recognition across multiple metrics, including classification accuracy and encoding sparsity. Additionally, we benchmark these methods against *Direct-SNN*, where CIR samples are fed directly into the SNN classifier, and against the six-layer CNN from [15] originally trained on Doppler spectrograms and retrained here on raw CIR data for a fair comparison. Computational efficiency is evaluated in terms of model size and average inference latency over ten runs, while spike activity rate serves as a proxy for energy consumption in neuromorphic hardware. These metrics provide insights into both effectiveness and practicality for deployment in resource-constrained environments. All the code is developed in Python, using the PyTorch and the snnTorch [5] frameworks.

A. Accuracy results

We compare the performance of the models on the test set using the *F1 score*, as it offers a more stable and reliable evaluation of the model performance when dealing with multiclass classification tasks over imbalanced datasets. To aggregate performance across classes, we employ the *macro-averaging* strategy, which calculates the F1 score independently for

Method	F1 score [%]	Params	Inference time [ms]	Spike rate [%]
SCAE-SNN	95.75 ± 1.18	2.8×10^4	$1.2 + 18.6$	10.7
CAE-SNN	95.16 ± 2.35	2.8×10^4	$0.7 + 18.7$	11.9
Delta thr. + SNN	74.59 ± 3.67	2.6×10^4	18.8	8.0
Direct-SNN-Lin	49.98 ± 3.83	6.7×10^4	24.4	8.5
Direct-SNN-Conv	19.45 ± 8.64	2.5×10^6	27.9	26.2
Baseline CNN [15]	85.87 ± 4.47	7.7×10^5	0.5	/

Table I: Performance comparison on the test set. F1 scores are reported as mean ± standard deviation over five weight initializations.

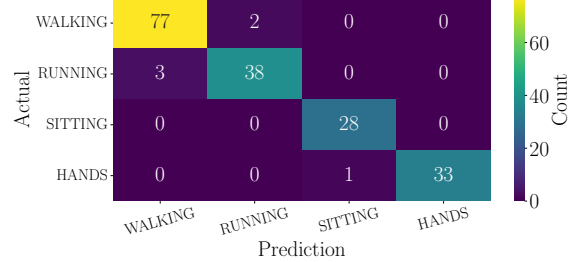


Figure 2: Confusion matrix of the SCAE-SNN model on the test set.

each class and then computes the arithmetic mean, ensuring equal contribution from all classes and a fair assessment of underrepresented ones. As shown in Table I, the SCAE-SNN and CAE-SNN models achieve comparable performance with F1 scores exceeding 95%, demonstrating their ability to generalize to unseen subjects (see Figure 2). The SNN trained on delta-threshold encoded data reaches approximately 75% F1 score, suggesting that a simple fixed threshold encoding is not sufficient for effective radar-based HAR. In contrast, direct training of an SNN on raw CIR samples results in markedly degraded performance (e.g., the Direct-SNN-Conv consistently predicts a single class) indicating limited capacity to extract discriminative spectral features. Furthermore, the baseline CNN from [15] exhibits a reduction of roughly ten percentage points in F1 score when retrained on raw CIR data compared to the results reported in the original paper, highlighting the superiority of the proposed spike-based architecture in learning directly from raw signals.

B. Sparsity of the encoding

We define the sparsity of a spike encoding as the fraction of zeros it contains. The sparsity directly correlates with the efficiency of the SNN: higher sparsity implies fewer computations, which translates into a lower energy consumption. As shown in Table II, our SCAE produces the sparsest spike encoding (over 81%), being approximately $2.8 \times$ sparser than the standard CAE ($\approx 29\%$) and notably sparser than the delta thresholding approach ($\approx 72\%$). This result indicates that our spike encoding can significantly reduce computational load and energy usage, while maintaining effective representations.

C. Computational efficiency

Our SCAE-SNN uses a compact architecture with 28 k parameters, making it one of the smallest models considered. For the first two architectures, the reported inference time in Table I corresponds to the sum of the encoding and classification stages, whereas other methods report only the

Encoding method	Sparsity
SCAE	81.1%
CAE	28.6%
Delta Thresholding	71.7%

Table II: Average sparsity of the encoding methods on the test set.

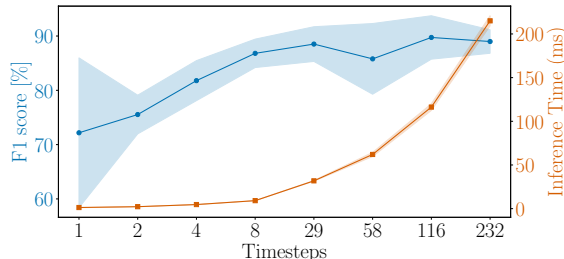


Figure 3: Inference time vs. F1 score across timesteps. Shaded areas represent \pm one standard deviation computed over ten seeds.

classification time. The SCAE-SNN achieves a total inference time of approximately 19.8 ms, which is slightly higher than the CAE-SNN, yet substantially lower than the Direct-SNN approaches, which perform only classification. Nevertheless, the higher encoding time is compensated for by the SCAE event-driven operation and high sparsity, which leads to fewer effective computations on neuromorphic hardware. In terms of spike activity, our method exhibits a firing rate of 10.7%, lower than CAE-SNN, confirming its computational efficiency and potential for energy savings.

D. Tradeoff between F1 score and inference time

The classification inference time is directly linked to the number of timesteps T and defines the temporal resolution of the model. Increasing T enables richer temporal dynamics and improved accuracy in capturing sequential dependencies, but at the cost of higher computational overhead. Reducing T improves efficiency, but may limit the network ability to fully exploit temporal information. Figure 3 shows the tradeoff between the classification inference time and the F1 score. As expected, a larger T leads to an increase in the F1 score, which however, tends to saturate after 29 timesteps. At the same time, the inference time grows proportionally, as the SNN must process the input over more timesteps. These results suggest that $T = 29$ represents a suitable choice for runtime deployment of the architecture.

VII. CONCLUDING REMARKS

In this paper, we proposed an end-to-end pipeline for radar-based HAR using SNNs, introducing a learned spike encoding tailored to raw CIR data, thus avoiding the need for costly Doppler domain preprocessing. The proposed architecture consists of a spiking convolutional autoencoder combined with an SNN classifier. The first learns to generate sparse spike trains that preserve human movement features, while minimizing spike activity for energy efficiency. The latter, instead, performs activity recognition directly from the encoded CIR data. The modules are jointly trained to balance reconstruction fidelity and classification accuracy. Experimental

results demonstrate that the proposed approach achieves high efficiency in terms of model size, inference time, and spike activity, without compromising accuracy, making it a practical solution for real-time deployment on resource-constrained devices. Future research will focus on extending the framework to multi-antenna systems, enabling richer spatial sensing, as well as evaluating the approach in multi-user ISAC scenarios.

REFERENCES

- [1] A. Shastri, N. Valecha, E. Bashirov, H. Tataria, M. Lentmaier, F. Tufvesson, M. Rossi, and P. Casari, “A review of millimeter wave device-based localization and device-free sensing technologies and applications,” *IEEE Comm. Surveys & Tutorials*, vol. 24, no. 3, pp. 1708–1749, 2022.
- [2] J. Pegoraro, J. O. Lacruz, F. Meneghelli, E. Bashirov, M. Rossi, and J. Widmer, “RAPID: Retrofitting IEEE 802.11ay Access Points for Indoor Human Detection and Sensing,” *IEEE Transactions on Mobile Computing*, pp. 1–18, 2023.
- [3] Y. Ma, G. Zhou, and S. Wang, “WiFi sensing with channel state information: A survey,” *ACM Computing Surveys (CSUR)*, vol. 52, no. 3, pp. 1–36, 2019.
- [4] S. Lahmer, A. Khoshirsat, M. Rossi, and A. Zanella, “Energy consumption of neural networks on Nvidia edge boards: an empirical model,” in *20th International Symposium on Modeling and Optimization in Mobile, Ad hoc, and Wireless Networks (WiOpt)*, pp. 365–371, IEEE, 2022.
- [5] J. K. Eshraghian, M. Ward, E. O. Neftci, X. Wang, G. Lenz, G. Dwivedi, M. Bennamoun, D. S. Jeong, and W. D. Lu, “Training spiking neural networks using lessons from deep learning,” *Proc. of the IEEE*, 2023.
- [6] C. Frenkel, M. Lefebvre, J.-D. Legat, and D. Bol, “A 0.086-mm² 12.7-pJ/SOP 64k-synapse 256-neuron online-learning digital spiking neuromorphic processor in 28-nm CMOS,” *IEEE Transactions on biomedical circuits and systems*, vol. 13, no. 1, pp. 145–158, 2018.
- [7] Y. Kim and H. Ling, “Human Activity Classification Based on Micro-Doppler Signatures Using a Support Vector Machine,” *IEEE Transactions on Geoscience and Remote Sensing*, vol. 47, no. 5, pp. 1328–1337, 2009.
- [8] X. Li, Y. He, and X. Jing, “A Survey of Deep Learning-Based Human Activity Recognition in Radar,” *Remote Sensing*, vol. 11, no. 9, 2019.
- [9] D. Banerjee, S. Rani, A. M. George, A. Chowdhury, S. Dey, A. Mukherjee, T. Chakravarty, and A. Pal, “Application of Spiking Neural Networks for Action Recognition from Radar Data,” in *2020 International Joint Conference on Neural Networks (IJCNN)*, pp. 1–10, 2020.
- [10] I. J. Tsang, F. Corradi, M. Sifalakis, W. Van Leeuwijk, and S. Latré, “Radar-Based Hand Gesture Recognition Using Spiking Neural Networks,” *Electronics*, vol. 10, no. 12, 2021.
- [11] M. Arsalan, A. Santra, M. Chmurski, M. El-Masry, G. Mauro, and V. Issakov, “Radar-Based Gesture Recognition System using Spiking Neural Network,” in *2021 26th IEEE International Conference on Emerging Technologies and Factory Automation (ETFA)*, pp. 1–5, 2021.
- [12] M. Arsalan, A. Santra, and V. Issakov, “Spiking Neural Network-Based Radar Gesture Recognition System Using Raw ADC Data,” *IEEE Sensors Letters*, vol. 6, no. 6, pp. 1–4, 2022.
- [13] E. Cicciarella, R. Mazzieri, J. Pegoraro, and M. Rossi, “Learned spike encoding of the channel response for low-power environment sensing,” in *2024 IEEE International Conference on Pervasive Computing and Communications Workshops (PerCom Workshops)*, pp. 763–768, 2024.
- [14] W. Gerstner, W. M. Kistler, R. Naud, and L. Paninski, *Neuronal dynamics: From single neurons to networks and models of cognition*. Cambridge University Press, 2014.
- [15] J. Pegoraro, P. Saucedo, J. O. Lacruz, M. Rossi, and J. Widmer, “DISC: A Dataset for Integrated Sensing and Communications in mmWave Systems,” *IEEE Communications Magazine*, vol. 63, no. 10, pp. 94–100, 2025.
- [16] L. Müller, M. Sifalakis, S. Eissa, A. Yousefzadeh, P. Detterer, S. Stuijk, and F. Corradi, “Aircraft Marshaling Signals Dataset of FMCW Radar and Event-Based Camera for Sensor Fusion,” in *2023 IEEE Radar Conference (RadarConf23)*, pp. 01–06, 2023.
- [17] E. O. Neftci, H. Mostafa, and F. Zenke, “Surrogate Gradient Learning in Spiking Neural Networks: Bringing the Power of Gradient-Based Optimization to Spiking Neural Networks,” *IEEE Signal Processing Magazine*, vol. 36, no. 6, pp. 51–63, 2019.